

From nanometers to gigaparsecs: The role of nanostructures in unraveling the mysteries of the cosmos

Mark L. Schattenburg^{a)}

*Space Nanotechnology Laboratory, Center for Space Research, Massachusetts Institute of Technology,
77 Massachusetts Avenue, Cambridge, Massachusetts 02139*

(Received 1 June 2001; accepted 24 September 2001)

High launch costs and the extreme distance to astrophysical objects place a premium on astrophysical instrumentation with the highest attainable sensitivity and resolution at the lowest possible weight and cost. Many interesting and useful optical phenomena occur when the size and placement accuracy of features are comparable to, or smaller than, the wavelength of light. These considerations have compelled us to develop a variety of nanotechnologies that have now been utilized in space physics instrumentation on nine missions. These include 200- and 400-nm-period membrane-supported transmission gratings for high-resolution spectroscopy of astrophysical x-ray sources, mesh-supported transmission gratings for solar extreme ultraviolet (EUV) monitoring, and UV nanofilters with 45 nm slots that are key components of atom cameras observing Earth's magnetosphere. This article will describe instruments on space missions where we have applied nanotechnology. One application is the NASA Chandra Observatory x-ray telescope, for which we manufactured a large quantity of transmission gratings for high-resolution spectroscopy. Chandra is now returning a torrent of high-quality x-ray images and spectra from such interesting objects as supernova remnants, the accretion disks around black holes and neutron stars, stellar coronae, galaxy cluster cooling flows, and other x-ray-emitting objects up to gigaparsecs distant. [A short astronomy lesson: As Earth orbits Sol, nearby stars in the sky appear to wobble due to parallax. At a distance of one parsec (a "parallax-second"), the diameter of Earth's orbit ($\sim 1.5 \times 10^{11}$ m) subtends one arcsecond, so a parsec is around 3.3 light years, or 3.1×10^{16} m. For reference, the nearest star is around a parsec away, our Milky Way galaxy is a few kiloparsecs across, nearby galaxies are megaparsecs away, and the known universe is measured in gigaparsecs (10^{25} m).] Another application is the atom "camera" on the NASA Imager for Magnetopause-to-Aurora Global Exploration (IMAGE) spacecraft that studies Earth's magnetosphere, the belt of plasma around the Earth formed by swept-up ions from the Solar wind trapped in the bottle of Earth's magnetic field. The camera images the magnetosphere in the "light" of neutral atoms, rather than photons, emitted from the plasma due to charge exchange processes. We developed nanofilters, consisting of 500-nm-thick gold foils with 45-nm-wide slots, that are designed to block unwanted deep-UV and EUV photons which would otherwise overwhelm the detector with a million-to-one noise-to-signal ratio, thus allowing the camera to detect the weak atom fluxes. IMAGE is now sending back spectacular atom movies of the magnetosphere revealing a wealth of new information about this complex and dynamic environment. Finally, I describe work in our laboratory aimed at developing microtechnology for the shaping and assembly of glass microsheet optics to few-nanometer accuracy. We believe these new x-ray optics will spawn a new generation of diffraction-limited x-ray telescopes with massive collecting areas and resolution approaching 0.1 microarcsecond (~ 1 picoradian). These new telescopes may enable the direct imaging of the massive black holes believed to lurk at the center of most galaxies. © 2001 American Vacuum Society. [DOI: 10.1116/1.1418410]

I. INTRODUCTION

Our universe is a bizarre place, filled with many mysterious and wonderful objects. There are supernova explosions that during their fury emit more energy than all the billions of stars in our galaxy combined. There are black holes and neutron stars, literally eating hapless normal stars like our sun, the superheated gas glowing brightly in x-rays as it is sucked down the deep gravitational wells. There are super-

massive black holes like the one believed to lurk at the center of our galaxy, many with more mass than all the stars in our galaxy combined and spraying huge jets of relativistic particles into space many times longer than our galaxy. These are just a sampling of the many strange objects under intensive study by astronomers around the globe.

These studies are shedding light on some of the central mysteries of the Universe: Why does only $\sim 10\%$ of the mass of the Universe appear to be visible? What is the nature of the mysterious "missing matter?" What powers the enormous relativistic jets shooting from quasars? (Massive black

^{a)}Electronic mail: marks@space.mit.edu

holes are suspected.) How did the universe get here and what is its ultimate fate?

Increasingly, astronomers are turning to space instrumentation to avoid the perturbing effects of the atmosphere and study wavelength bands otherwise inaccessible. There has been a great deal of recent interest in the application of micro and nanotechnology to space hardware. This interest is natural given the extreme need for spacecraft systems miniaturization due to astronomically high launch costs and the urgent need for “smart” materials and systems that can perform in hostile environments far from human support or repair. Much of this work has focused on such micro-electromechanical systems (MEMS) devices as microthrusters, sensors, and actuators. Nanotechnology for advanced materials and biological applications are also of great interest to the space community.

Our laboratory has concentrated on developing micro and nanotechnology for space physics instrumentation. This technology has been applied to a variety of missions ranging from x-ray astronomy telescopes, which study objects as far as the edge of the known universe, to instruments studying nearby plasmas around the Sun and Earth. In general, our efforts have focused on solving particularly challenging space optics problems in the UV and x-ray bands, where a specific optical task needs to be performed with maximum optical performance and minimum weight.

Nanofabricated optical components developed in our laboratory can generally be characterized as passive structures marked by a high degree of accuracy, organization, and dimensional control. For example, of importance are gratings with precise control of period and line geometry, and very low levels of defects (pinholes). We have developed, adopted, or adapted a variety of nanofabrication tools to fabricate these structures, including methods of nanolithography, high-fidelity pattern transfer, nanometrology, and micro-electromechanical systems (MEMS) processing.

Typical nanofabricated structures for space instrumentation utilize extremely thin and flimsy components that must be accurately registered, and yet at the same time need to survive the extreme stresses of rocket vibration and the large thermal excursions typical of spacecraft environments, without risk of failure or compromise to accuracy. The interface of flimsy and precisely placed nanostructures with massive spacecraft structural members, in an environment of large mechanical and thermal disturbances, is what we call the scaling problem. This problem is generally solved by utilizing a scaled hierarchy of micromechanical supports that are eventually mated to robust spacecraft components using epoxy bonding and single-point and/or kinematic mounting schemes. The use of low-outgassing epoxies and well matched, low-thermal-expansion materials are also very important. Extensive finite-element modeling and environmental testing are essential to confirm component survivability. Fortunately, nanostructures are typically fabricated in the form of thin membranes and/or have such small members that their mechanical resonances are safely above the peak of typical rocket acoustic spectra.

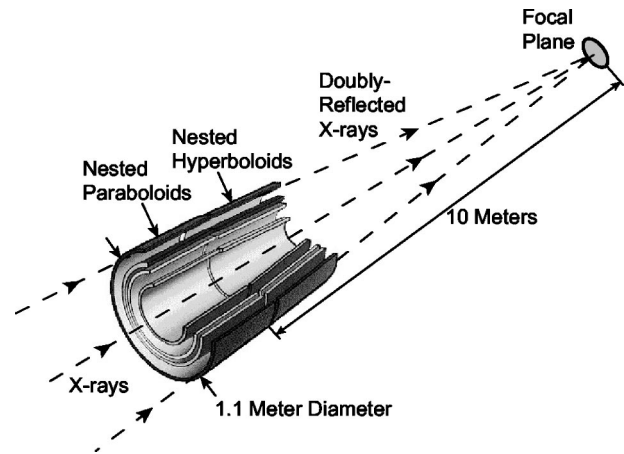


FIG. 1. Chandra x-ray telescope utilizes grazing-incidence optics of the Wolter I design. X rays bounce first from paraboloids of revolution and then from hyperboloids. The telescope collecting area is increased by the use of four nested shell pairs.

II. NANOTECHNOLOGY FOR SPACE MISSIONS

This section describes details of the instrumentation on nine space missions for which our laboratory has developed nanotechnology. Nanotechnology for future missions is described in Sec. III. In this article I use the encompassing term nanotechnology to describe structures with features in the sub-100 nanometer range, and also larger features in the micrometer range where placement accuracy in the few nanometer range is required.

A. The Chandra Observatory x-ray telescope: Gratings for high-resolution x-ray spectroscopy

The Chandra Observatory is a large NASA x-ray telescope that was launched into Earth orbit by the Space Shuttle in July of 1999. Chandra is providing astrophysicists with high-resolution x-ray imaging and spectroscopy of astrophysical sources in the 0.1–10 keV energy band (wavelengths between 0.1 and 14 nm).^{1,2} Chandra utilizes grazing-incidence reflective optics of the Wolter I design to image x rays (see Fig. 1). X rays experience two reflections to focus, bouncing first from paraboloids of revolution and then from hyperboloids. Four nested shell pairs are used in order to increase collecting area. At the focal plane are two selectable imagers: a microchannel plate detector and a charge coupled device (CCD) camera.

In astronomy, imaging and spectroscopy are complementary and indispensable tools. High-resolution spectroscopy is a particularly powerful tool in the x-ray band for the study of hot plasmas. The universe is filled with a plethora of bizarre objects harboring plasmas in the one- to ten-million-degree temperature range that emit bright and richly detailed x-ray spectra. Examples of these objects are the shock waves of supernova explosions and the accretion disks surrounding black holes and neutron stars that orbit and consume normal stars. Initial results from Chandra confirm the value of high-resolution x-ray spectra and reveal a wealth of information about such plasmas, including temperatures, element abundances, velocities, and ionization lifetimes.^{3–5}

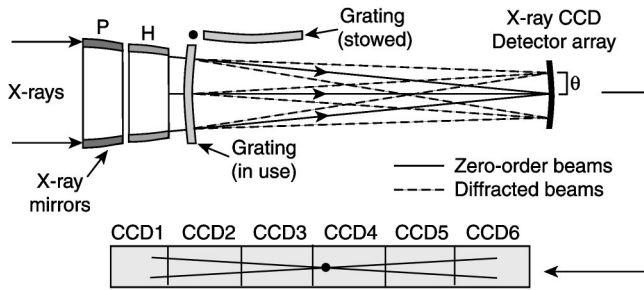


Fig. 2. Optical design of the high energy transmission grating spectrometer (HETGS). X rays are focused through the grating disk and dispersed into an X-shaped spectrum across a row of x-ray CCD detectors.

On Chandra, two instruments provide high-resolution spectroscopy. The low energy transmission grating spectrometer (LETGS), built by the Space Research Organization Netherlands (SRON), uses $1.0\ \mu\text{m}$ -period gold transmission gratings for spectroscopy in the $0.15\text{--}14\ \text{nm}$ wavelength band,^{6,7} while the high energy transmission grating spectrometer (HETGS), built by MIT, uses 200 and 400 nanometer-period gold transmission gratings, fabricated in our laboratory, for spectroscopy in the $0.15\text{--}3\ \text{nm}$ wavelength band.⁸

The optical principal of the HETGS is depicted in Fig. 2. X rays reflecting from the telescope mirrors are focused through the grating array and dispersed along an imager consisting of a row of six CCD chips, also made by MIT.⁹ On the detector, short wavelengths land near the zero-order image while long wavelengths land farther away. In order to provide coverage of the extremely large telescope bandwidth, the outer-two optic shells are mounted with gratings that provide double the dispersion of those used with the inner two. Spectral overlapping is avoided by mounting the two grating sets offset by a small angle, such that the spectra forms a shallow “X” on the detector.

A photograph of the HETGS and an individual grating element are shown in Fig. 3. The spectrometer consists of a 1.1-m-diameter toroidal aluminum disk in a Rowland circle geometry, to which are mounted 196 gratings with 400 nm period (MEGs) and 144 gratings with 200 nm period (HEGs). Gold grating lines are supported by submicron-thickness polyimide membranes bonded to Invar frames (see Fig. 4). The grating bars are designed to provide $\sim\pi$ phase shift of the transmitted x rays, maximizing first-order efficiency [Fig. 4(b)]. The spectral resolution goal of $\lambda/\Delta\lambda > 1000$ at the 1 nm wavelength placed stringent limits on the allowable magnitude of grating period and rotation errors. To achieve this goal, all gratings were required to have the same period to within 250 parts per million and to be rotationally aligned to within 1 arc min. The use of frames made of low-thermal-expansion Invar metal, in conjunction with a single-point cantilevered mounting scheme [mounting tab visible in Fig. 3(b)] were essential to control mounting distortions.

The high resolution and efficiency of the HETGS enable scientists to obtain x-ray spectra of unprecedented quality.

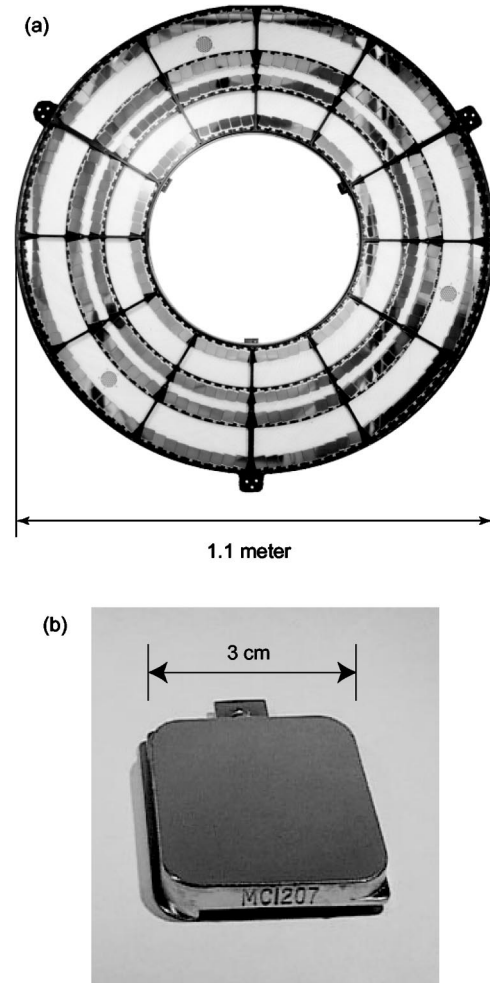


Fig. 3. (a) Photograph of the HETGS disk to which are mounted 340 grating facets. (b) Photograph of individual grating facet.

Figure 5 depicts the spectra of the x-ray binary star Capella.³ Narrow fluorescent emission lines from highly ionized silicon, magnesium, neon, iron, and oxygen are visible in the spectra, the narrowness due to the tight control of the grating period during manufacturing.

The gratings were patterned by interference lithography (IL) as depicted in Fig. 6. Our IL system represents over 20 years of continuous development and has been highly optimized for high volume, high yield grating production. A beam from a $\lambda=351.1\ \text{nm}$ argon ion laser is split into two beams, expanded by spatial filters, and then recombined with intersection angle 2Θ . The resulting standing-wave grating image, with period $p=\lambda/(2\sin\Theta)$, is captured in a photosensitive resist. Active fringe-locking optoelectronics establish a high-contrast grating image.

A macroview of the fabrication process is depicted in Fig. 7. Details of our fabrication process are available elsewhere.¹⁰ In the first step [Fig. 7(a)], 100-mm-diameter silicon wafers are coated with $0.5\text{--}1.0\ \mu\text{m}$ of polyimide, which will later form the support membrane, a plating base consisting of 5 nm of chromium and 20 nm of gold, and a trilayer resist consisting of $0.5\text{--}1.0\ \mu\text{m}$ of antireflection coat-

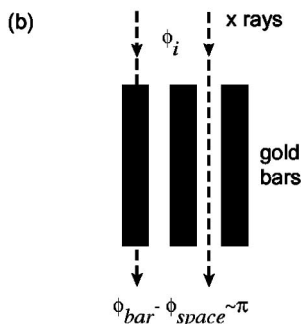
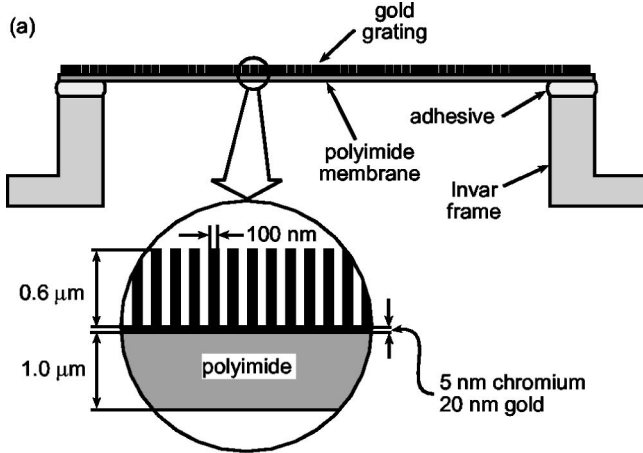


FIG. 4. (a) Design of HETGS x-ray transmission grating element (HEG type). The polyimide support membrane is substantially transparent to the x-ray band of interest. (b) Depiction of π -phase shifting principle of x-ray transmission gratings, which suppresses zero order and maximizes first-order efficiency.

ing (ARC), 15 nm of tantalum pentoxide, and 200 nm of resist. Our group was the first to apply ARC and trilayer resist processing to IL.¹¹ In the second step [Fig. 7(b)], the trilayer resist is patterned by IL and converted to gold using

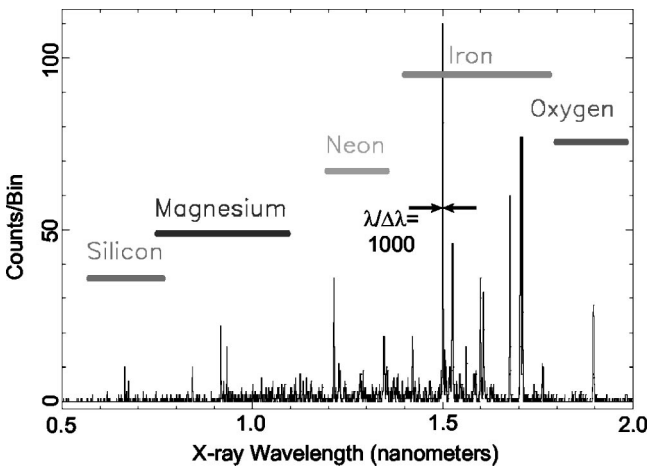


FIG. 5. Chandra telescope HETGS spectra of the x-ray binary star Capella (Ref. 3). Astrophysical plasmas in the $(1-10) \times 10^6$ degree range emit bright fluorescent spectra in the 0.1–10 nm wavelength band, revealing a wealth of detailed information.

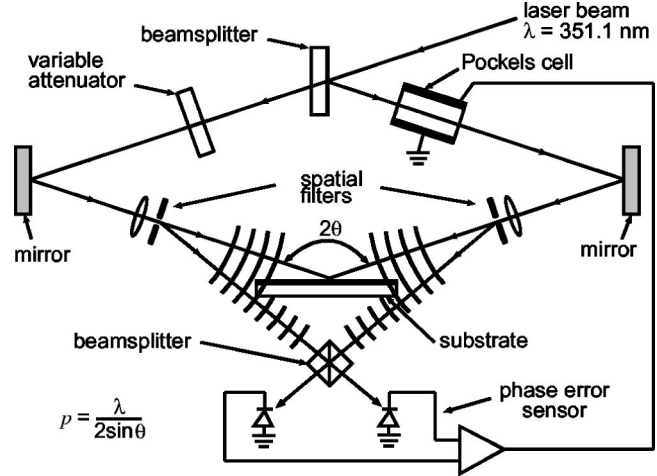


FIG. 6. Depiction of interference lithography. A UV laser beam is split into two beams, the beams then expanded and crossed to recombine. The interfering beams create a standing wave grating pattern that is captured by a resist-coated substrate. Active fringe-locking electronics suppresses the effects of vibration and turbulence.

a process described in more detail below and depicted in Fig. 8. In the third step the substrate is spin etched from the backside using an HF/HNO₃ mixture, stopping on the polyimide layer [Fig. 7(c)].¹² Finally, an Invar frame is aligned and bonded to the resulting membrane [Fig. 7(d)] and the frame is cut out [Fig. 7(e)].

A microview of the fabrication process is depicted in Fig. 8. First the substrates are coated with the six layers described previously [Fig. 8(a)] and then patterned by IL [Fig. 8(b)]. Next the resist is used as a mask to etch into the interlayer by CF₄ RIE [Fig. 8(c)], and subsequently the interlayer is used as a mask to etch into the ARC by oxygen RIE [Fig. 8(d)]. The resulting polymer form is used as a mold for gold electroplating [Fig. 8(e)], followed by stripping of the interlayer and ARC [Fig. 8(f)]. Finally the substrate is spin etched from the backside and the resulting membrane is bonded to a metal frame as described previously [Fig. 8(g)].

Electron micrographs of intermediate steps in the fabrication process are shown in Fig. 9. The resist after interference

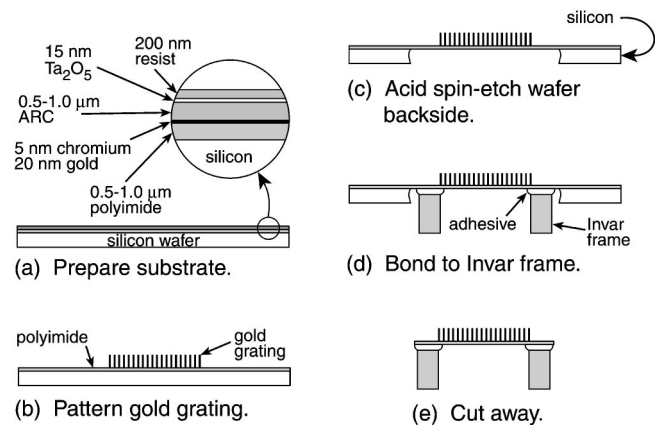


FIG. 7. Membrane-supported transmission grating fabrication process (macroview).

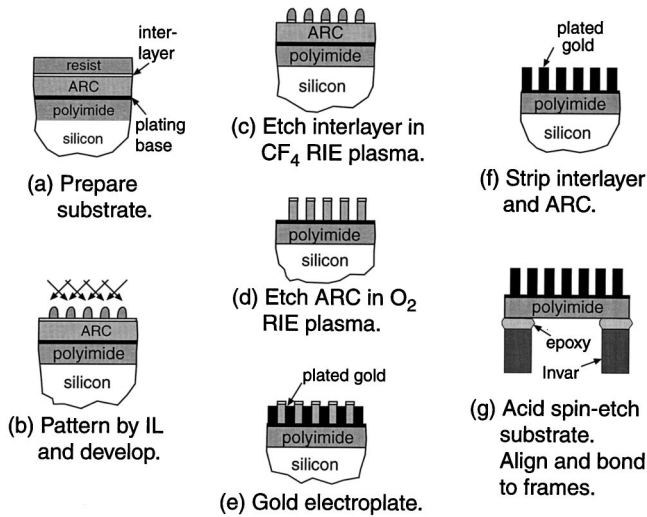


FIG. 8. Membrane-supported transmission grating fabrication process (microview).

lithography and development is shown in Fig. 9(a), the ARC after oxygen RIE down to the plating base is shown in Fig. 9(b), and the gold grating after ARC stripping is shown in Fig. 9(c).

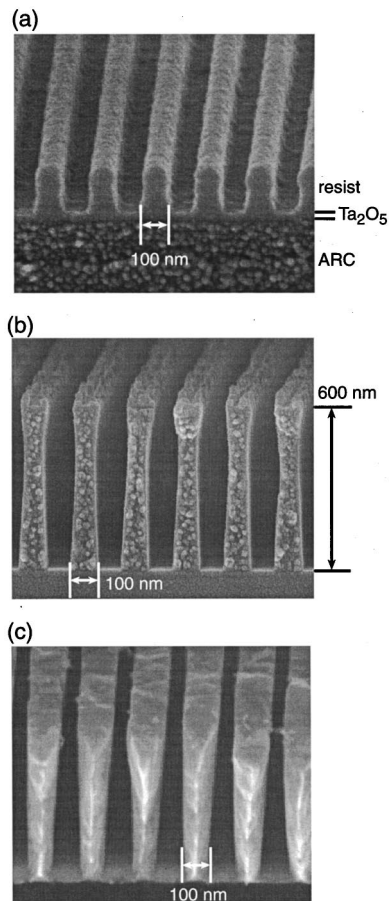


FIG. 9. Electron micrographs of intermediate transmission grating processing steps. (a) Resist after interference lithography. (b) ARC after oxygen RIE down to plating base. (c) Gold grating lines after electroplating and resist stripping.

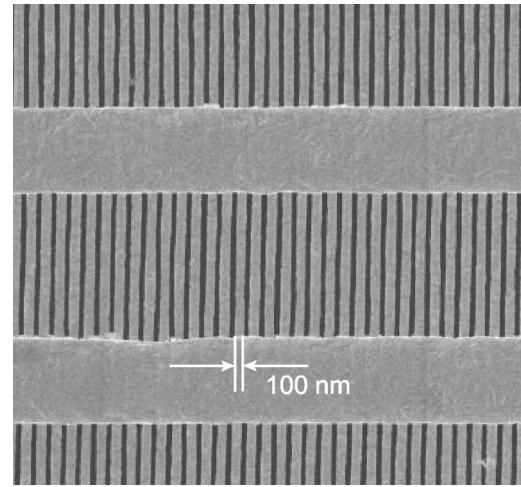


FIG. 10. Mesh-supported gold transmission grating for solar EUV monitoring.

B. The SOHO and GOES missions: Gratings for solar UV/EUV monitoring

The NASA/ESA Solar and Heliospheric Observatory (SOHO) was launched in December 1995. Our laboratory fabricated 200-nm-period gold transmission gratings for the Solar EUV monitor (SEM), built by the University of Southern California and International Radiation Detectors Corp., which monitors the Solar extreme ultraviolet (EUV) $\lambda=30.4$ nm He II line.^{13,14} In the EUV and soft x-ray bands the polyimide support membranes used for the Chandra gratings are opaque and need to be avoided. Additional fabrication steps were utilized for the SOHO gratings to pattern, using contact lithography, an integral gold support mesh over the 200-nm-period grating, consisting of a 4.0- μm -period grating crossed with a 150- μm -period grating (see Fig. 10).

More recently we developed a much stronger integral nickel honeycomb support mesh using contact and interference lithographies to produce gold transmission gratings for UV/EUV spectrometers on the NASA/NOAA Geostationary Operational Environmental Satellites (GOES) N, O, P, and Q missions, planned for launch in 2002, 2005, 2007, and 2010. The spectrometers, built by Panametrics and International Radiation Detectors Corps., will monitor four solar EUV bands between $\lambda=8-100$ nm and the hydrogen Lyman alpha wavelength at 121.6 nm. We fabricated gratings with 200, 400, and 600 nm periods using a process described in Sec. II C. The Solar instruments will help understand, and perhaps give advanced warning of, solar storms that can damage satellites and endanger astronaut health.

C. The IMAGE and TWINS missions: Nanofilter gratings for neutral atom imaging of Earth's magnetosphere

The NASA Imager for Magnetopause-to-Aurora Global Exploration (IMAGE) satellite, launched by NASA in March 2000, uses an arsenal of instruments to study Earth's magnetosphere.^{15,16} The magnetosphere is the belt of plasma around the Earth formed by swept-up ions from the Solar

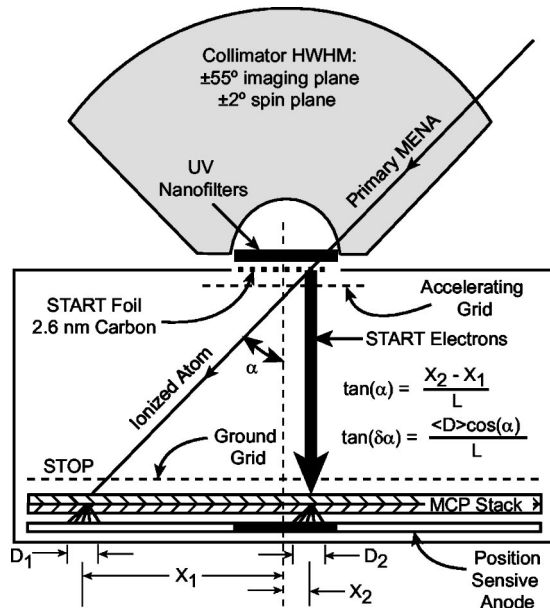


FIG. 11. IMAGE mission medium energy neutral atom (MENA) camera instrument concept. At the bottom of the detector a microchannel plate (MCP) stack, backed by a position-sensitive anode (PSA), amplifies and senses charged particles. Energetic neutral atoms (ENAs) are first collimated and then ionized by a 2.6-nm-thick carbon foil. An accelerating grid produces a pulse of electrons on the PSA and starts a clock. The position and time of the ion hitting the PSA allows measurement of the direction and energy, respectively, of the primary ENA. UV nanofilters prevent deep-UV photons from flooding the detector.

wind trapped in the bottle of Earth's magnetic field. This complex magnetohydrodynamic environment can change dramatically as the Earth is buffeted by powerful solar storms, giving rise to a variety of phenomena, dubbed "space weather." The aurora borealis or "northern lights" is one manifestation of these geomagnetic storms. Space weather is of great interest to the space community since these storms are a danger to satellites and astronauts.

Traditional methods of magnetospheric study have been limited to sending space probes through this region and attempting to deduce its complex onionskin structure from point measurements of plasma density. New instruments on IMAGE have enabled, for the first time, the direct high-resolution imaging of the magnetosphere in the "light" of neutral atoms, rather than photons, emitted from the plasma due to charge exchange processes.¹⁷ Energetic neutral atoms (predominantly oxygen) are created when ions, trapped and spiraling in Earth's magnetic field, collide with neutral hydrogen atoms in Earth's tenuous geocorona. The ion captures an electron from the hydrogen atom, forming an energetic neutral atom (ENA) that subsequently leaves the magnetosphere, while the hydrogen atom becomes ionized and takes its place in the trap. These neutral atoms contain direct information about the composition, energy, and density of the target plasma population. IMAGE is now sending back spectacular atom images of the magnetosphere that reveal a wealth of new information about this dynamic environment.

The medium energy neutral atom (MENA) instrument on IMAGE, built by the Southwest Research Institute (SWRI)

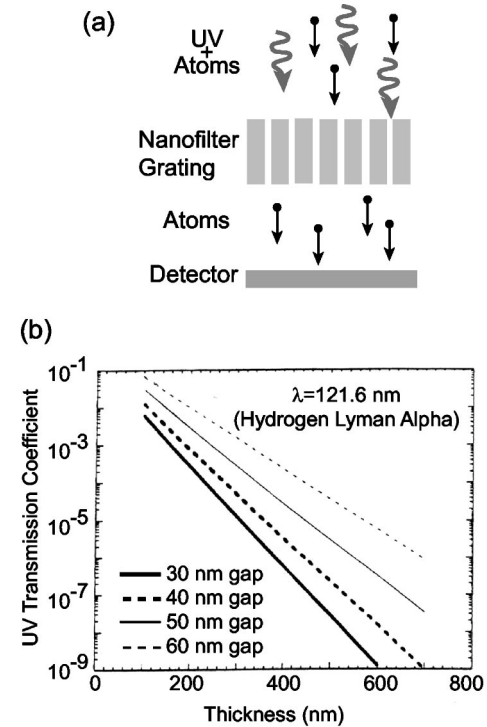


FIG. 12. (a) Depiction of nanofilter concept. (b) Results of model predictions for deep-UV transmission coefficient of nanofilter grating (Ref. 20).

and Los Alamos National Laboratory (LANL), is sensitive to ENAs in the 1–30 keV range.¹⁸ The MENA imager is a time-of-flight slit camera that utilizes a collimator array and spacecraft spin to produce images with $8^\circ \times 4^\circ$ angular resolution over a $140^\circ \times \sim 360^\circ$ field of view (see Fig. 11). ENAs entering the detector are collimated by a set of plates and then ionized by traversing a 2.5-nm-thick carbon foil. An accelerating grid produces a pulse of electrons that starts a clock. A segmented position-sensitive anode then determines the polar angle of the ENA from the position of the ion and its energy from the time of flight.

Unfortunately, this class of detectors suffers from a debilitating noise problem due to the intense and ubiquitous deep-UV radiation, predominantly hydrogen Lyman alpha ($\lambda = 121.6$ nm), originating from the Sun and scattered by Earth's atmosphere, which overwhelms the sensitive detector with a million-to-one noise-to-signal ratio. We developed nanofilter gratings, consisting of 500-nm-thick gold foils with 45-nm-wide slots, that are designed to block unwanted deep-UV and EUV photons, thus allowing the camera to detect the weak atom fluxes [see Fig. 12(a)]. The position of the filters in the instrument is visible in Fig. 11, between the collimator and carbon foil. The narrow slots in the nanofilters allow atoms to stream through while blocking deep-UV with a discrimination exceeding 10^6 , which has been confirmed by extensive modeling and measurement [Fig. 12(b)].^{19,20} These studies show that control over grating slot geometry is particularly critical: every 10 nm growth of slot width degrades the ability of the filter to block deep-UV by a factor of 10.

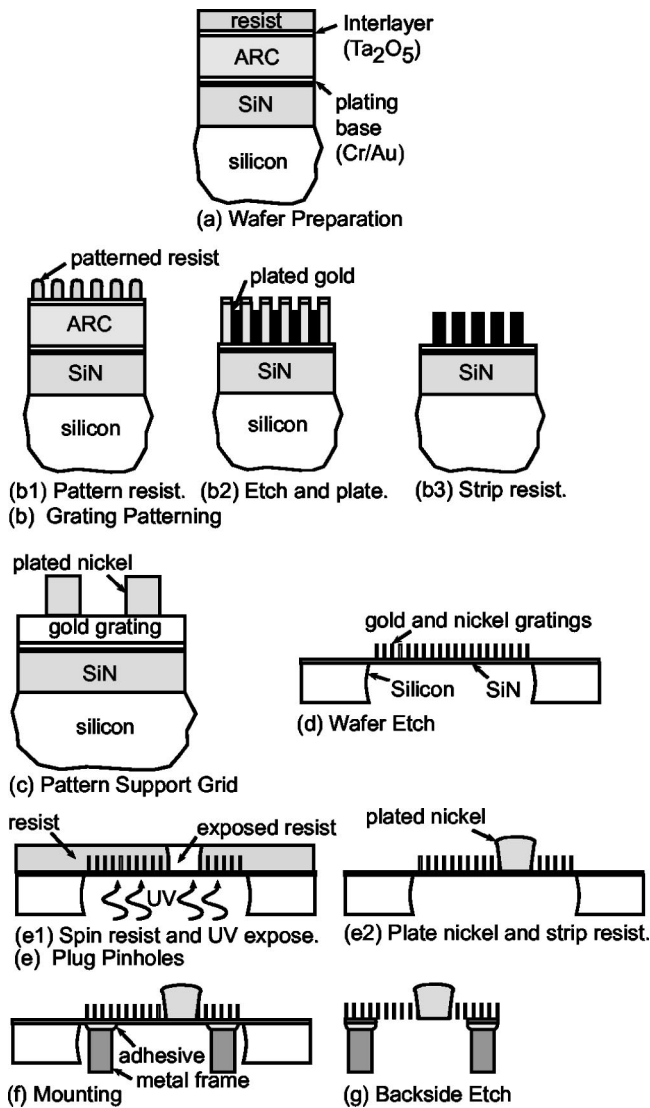


FIG. 13. Mesh-supported transmission grating fabrication process.

Nanofilters are much more difficult to fabricate than the Chandra gratings. The sub-45 nm slot width, the requirement that gratings are free standing to allow atom transmission, the need of a robust nickel support mesh which requires a nitride etch barrier, and the need for extremely low defect levels to prevent UV leakage, almost double the number of process steps, many of which are extremely unforgiving and required extensive development.

Our nanofilter fabrication process is depicted in Fig. 13. Details of our fabrication process are available elsewhere.²¹ First the substrates are coated with six layers similar to the Chandra gratings, except that low-stress silicon-rich nitride is substituted for polyimide [Fig. 13(a)]. The sacrificial nitride will later serve as a durable etch-stop barrier during HF/HNO₃ spin etching. The resist is then patterned by interference lithography (IL), the trilayer resist is wet and plasma developed, the lines are electroplated with gold, and the resist stripped, using processes similar to the Chandra gratings [Figs. 13(b1)–13(b3)]. The target ARC linewidth of 45 ± 3 nm was achieved through precise control of resist dose dur-

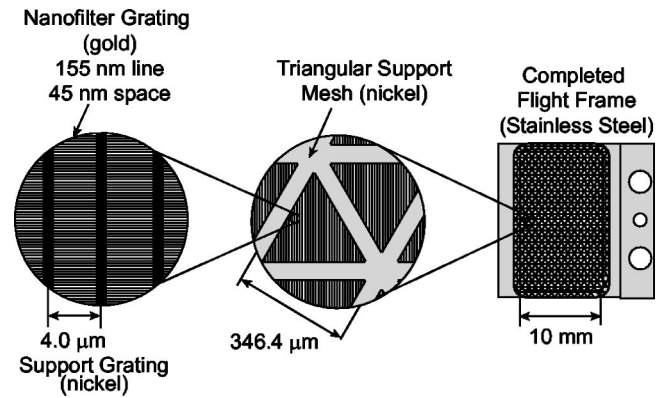


FIG. 14. Support mesh design for freestanding nanofilter transmission grating. (Left) Nanofilter grating and 4.0- μm -period nickel supporting grating. (Middle) Expanded view showing 4.0- μm -period nickel support grating and 346.4- μm -period nickel triangle-grid support mesh. (Right) Expanded view showing 346.4- μm -period nickel triangle mesh and stainless steel flight frame. Note the single-side cantilevered mounting scheme.

ing lithography and substrate temperature during RIE. Then additional resist is spun over the gold grating and a combination of IL and contact lithography is used to pattern an integral nickel support mesh consisting of a 4.0- μm -period grating and a 346.4- μm -period triangle grid [Fig. 13(c)]. Details of the support mesh design are depicted in Fig. 14. The wafer is then spin-etched from the back, stopping on the nitride barrier layer [Fig. 13(d)].

At this point an optional pinhole-plugging step is performed [Figs. 13(e1) and 13(e2)]. While pinholes are not a tremendous problem for gratings intended for spectroscopy, for the nanofilter gratings even a single 20 μm pinhole per square centimeter will leak well over one part per million of UV. We developed a simple self-plugging procedure that involves spinning resist over the grating and backlighting with actinic UV radiation [Fig. 13(e1)], followed by resist development and nickel electroplating [Fig. 13(e2)].

The grating membrane is then bonded to stainless steel frames and cut out, similar to the Chandra gratings [Fig. 13(f)]. Finally the nitride barrier and plating base are removed by plasma etching [Fig. 13(g)].

Electron micrographs of intermediate steps in the fabrication process are shown in Fig. 15. The ARC lines after lithography and oxygen RIE are shown in Fig. 15(a), and a top view of the gold grating after plating and ARC stripping is shown in Fig. 15(b).

We also fabricated similar gratings for two additional neutral-atom cameras: the NASA Two Wide-Angle Neutral-Atom Spectrometers (TWINS), scheduled for launch in 2002 and 2003, which will provide stereoscopic images of the magnetosphere.

The MENA camera on IMAGE is now sending back spectacular atom “movies” of geomagnetic storms. Figure 16 shows two frames from a movie of the magnetic storm of August 12, 2000. A huge blob of plasma has been deposited on the dark side of the earth, which over 12 h has spread around the equator in a so-called ring current.²² During storms as much as a million amperes can flow in these cur-

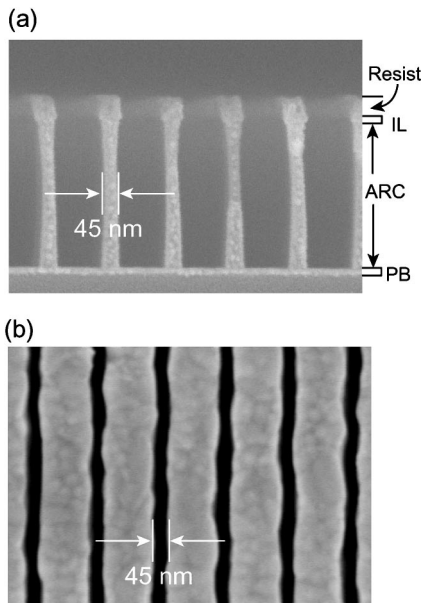


FIG. 15. Electron micrographs of nanofilter fabrication process steps. (a) Cleaved ARC after oxygen RIE. (b) Gold lines after plating and stripping.

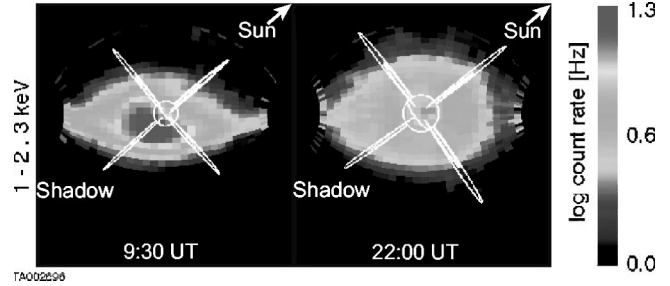
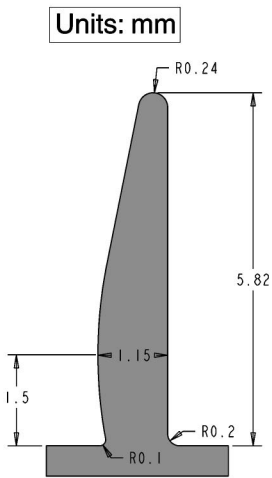


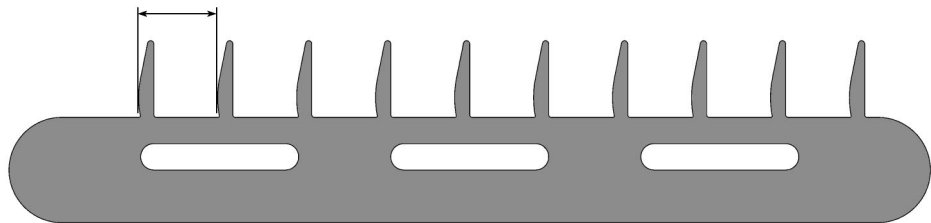
FIG. 16. Frames taken 12.5 h apart from an atom camera "movie" of the magnetospheric storm of August 12, 2000 (Ref. 22). The small white circle depicts Earth while the white loops are magnetic field lines. The view in the frames is from a pole with the Sun side of the Earth in the upper right hand corner and the night side in the lower left.

rents, inducing similar currents in long transmission lines and pipelines on the Earth. Intense magnetic storms have been known to destroy satellites and have even knocked out the North American power grid.²³

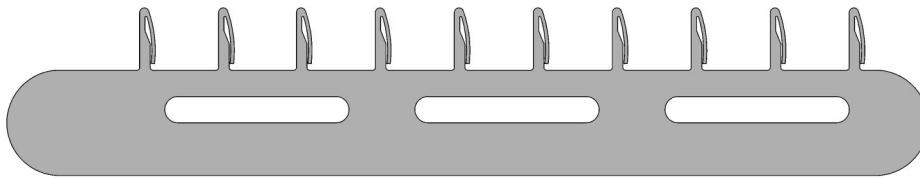
Two Types of Silicon Micro-Combs



Spacing tolerances << 1 μm.



(a) Reference combs are designed to accommodate the mirror foils with ease and make highly accurate single-point contacts with the foils.



(b) Spring combs have flexible springs that impart minute forces to the foils to properly shape and position them.

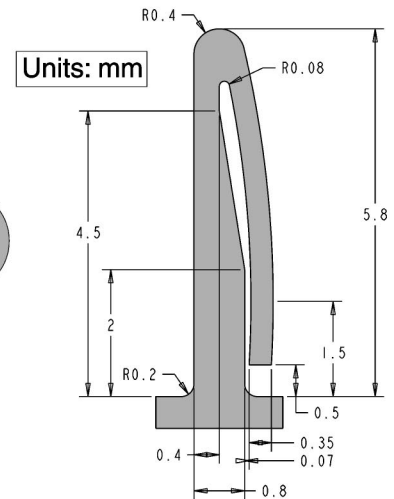


FIG. 17. Silicon microcomb design. (a) Reference combs are designed to make highly accurate single-point contact with x-ray mirror foils. (b) Spring combs have flexible springs that impart minute forces to properly shape and position foils.

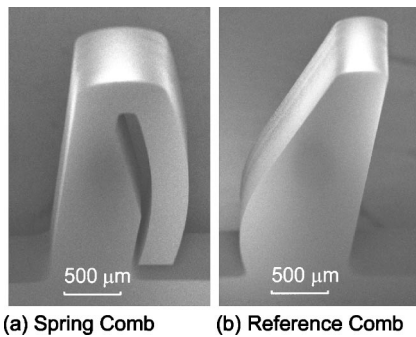


FIG. 18. Electron micrographs of microcombs. (a) Spring comb. (b) Reference comb.

III. NANOTECHNOLOGY FOR FUTURE SPACE MISSIONS

A number of new nanotechnologies are under development in our laboratory for possible use in future space missions, including the NASA Constellation X and MAXIM missions. These include 100-nm-period gold transmission gratings fabricated by achromatic interference lithography,²⁴ super-smooth x-ray reflection gratings,²⁵ and scanning-beam interference lithography that will lead to new high-resolution gratings with unprecedented control of period and phase.^{26,27} This last section will describe silicon microcomb technology that we have pioneered for the nano-accurate assembly of foil x-ray optics.

Traditional x-ray optics, such as depicted in Fig. 1, are generally fabricated by the extremely expensive and laborious method of cutting out the optic shells from huge blocks of low-expansion glass, followed by painstaking polishing. For example, the superb optics on Chandra achieve subarcsecond resolution, but at a cost well in excess of 100 million dollars and yet yielding little more effective collecting area than an amateur telescope. A number of groups worldwide are developing alternative foil optic designs based on glass microsheets only a few hundred microns thick, which are nested by the hundreds to provide large effective areas with very little mass.²⁸ Unfortunately, these groups have not been able to simultaneously achieve both large collecting area and high resolution, due to the difficulty of shaping and assembling thin foils to the required submicron tolerances. We are addressing these issues with micromachined structures.

Our microcomb design is depicted in Fig. 17. They consist of two types: reference combs [Fig. 17(a)] and spring combs [Fig. 17(b)]. The combs are CAD designed and then fabricated by lithographic patterning and etching all the way through silicon wafers, in cookie cutter fashion, using the Bosch plasma etch process.²⁹ Electron micrographs of completed combs are shown in Fig. 18.

The combs are used to establish a metrology reference frame in a piece of tooling called an assembly truss.^{30,31} The assembly truss utilizes a high-accuracy reference block, such as a flat or cylinder, to which the ends of all reference combs are registered. Because the combs are lithographically defined, all their surfaces are accurate to a small fraction of a micron. The reference block and the comb design accurately

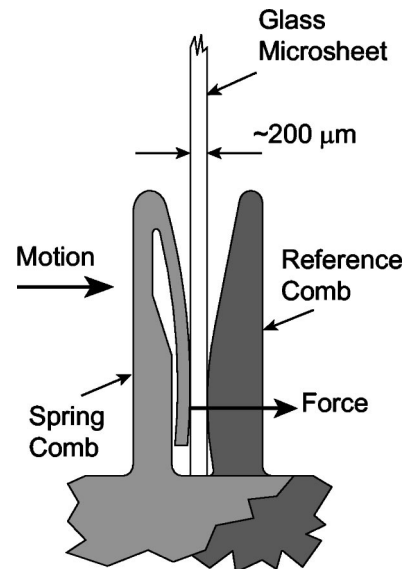


FIG. 19. Depiction of silicon microcomb assembly principle. Combs are designed to assemble $\sim 200\text{-}\mu\text{m}$ -thickness glass microsheets in a special piece of alignment tooling called an assembly truss. Spring combs are designed to slide in the assembly truss, forcing the microsheets against the fixed reference combs.

establish the contact surfaces of all the reference comb teeth to precisely position the foils to their correct locations and shapes in three-space. The spring combs are designed for sliding actuation in the assembly truss, so that the spring teeth apply controlled amounts of force to nudge the foils against the reference teeth (see Fig. 19). We have built and tested an assembly truss that has demonstrated submicron assembly accuracy, corresponding to subarcsecond optical quality.³⁰ This represents a $\sim 100\times$ improvement over previous foil optic assembly technology.³²

The short wavelength of x-rays potentially enables a 1000-fold improvement in resolution over visible light telescopes, but diffraction-limited performance has been difficult to achieve. As lithographic accuracy improves over the next decade, one could imagine fabricating microcombs with dimensional tolerances approaching 10 nm. It turns out that this is the required figure and assembly tolerance for fabricating diffraction-limited optics for $\lambda=1$ nm x rays, due to the tremendous $\sin(\Theta)$ relaxation of optic figure tolerance at grazing angles.³³ A proposed NASA mission, the Micro Arc-second X-ray Imaging Mission (MAXIM),³⁴ may perhaps utilize x-ray interferometer optics based on silicon microcomb assembly. If MAXIM can be realized, telescope resolutions of 1 picoradian (0.1 microarcsecond) will become possible, some 10^6 times better than conventional telescopes. Such a resolution would enable the direct imaging of the supermassive black holes believed to lurk at the center of galaxies.

ACKNOWLEDGMENTS

Words cannot express the author's profound sense of gratitude to Professor Claude R. Canizares and Professor Henry I. Smith for their unwavering support and encourage-

ment these past two decades. The author must also acknowledge the invaluable contributions of a large number of dedicated scientists, engineers, students, technicians, and research staff from MIT and other institutions around the country, and express regret at not being able to thank them individually. The support of the National Aeronautics and Space Administration, Los Alamos National Laboratory, Southwest Research Institute, and the Defense Advanced Research Projects Administration are also gratefully acknowledged.

- ¹M. Weisskopf, S. L. O'Dell, and L. P. VanSpeybroeck, *Proc. SPIE* **2805**, 2 (1996).
- ²M. Weisskopf, B. Brinkman, C. Canizares, G. Garmire, S. Murray, and P. VanSpeybroeck, *Pub. Astron. Soc. Pac.* (in press).
- ³C. R. Canizares, D. S. Huenemoerder, D. S. Davis, D. Dewey, K. A. Flanagan, J. Houck, T. H. Markert, H. L. Marshall, M. L. Schattenburg, N. S. Schulz, M. Wise, J. J. Drake, and N. S. Brickhouse, *Astrophys. J.* **539**, L41 (2000).
- ⁴C. R. Canizares, K. A. Flanagan, D. S. Davis, D. Dewey, J. C. Houck, and M. L. Schattenburg, in *Young Supernova Remnants: Eleventh Astrophysics Conference, College Park, Maryland, 2000*, AIP Conf. Proc. 565, edited by S. S. Holt and U. Hwang (AIP, Melville, NY, 2001), pp. 213–221 (press).
- ⁵K. A. Flanagan, C. R. Canizares, D. S. Davis, D. Dewey, J. C. Houck, and M. L. Schattenburg, in *X-Ray Astronomy 2000*, edited by R. Giacconi, S. Serio, and L. Stella, ASP Conf. Proc. 234 (Astronomical Society of the Pacific, San Francisco, in press).
- ⁶P. Predehl, H. Brauning, A. C. Brinkman, D. Dewey, J. J. Drake, K. A. Flanagan, T. Gunsing, G. D. Hartner, J. Z. Juda, M. Juda, J. Kaastra, H. L. Marshall, and D. Swartz, *Proc. SPIE* **3113**, 172 (1997).
- ⁷A. C. Brinkman, C. J. Th. Gunning, J. S. Kaastra, H. Brauning, G. Hartner, P. Predehl, J. J. Drake, J. Z. Juda, M. Juda, D. Dewey, K. A. Flanagan, and H. L. Marshall, *Proc. SPIE* **3113**, 181 (1997).
- ⁸T. H. Markert, C. R. Canizares, D. Dewey, M. McGuirk, C. Pak, and M. L. Schattenburg, *Proc. SPIE* **2280**, 168 (1994).
- ⁹M. W. Bautz *et al.* *Proc. SPIE* **3444**, 210 (1998).
- ¹⁰M. L. Schattenburg, R. J. Aucoin, R. C. Fleming, I. Plotnik, J. Porter, and H. I. Smith, *Proc. SPIE* **2280**, 181 (1994).
- ¹¹M. L. Schattenburg, R. J. Aucoin, and R. C. Fleming, *J. Vac. Sci. Technol. B* **13**, 3007 (1995).
- ¹²M. L. Schattenburg, R. I. Fuentes, G. Czernienko, R. C. Fleming, and J. Porter, *Mater. Res. Soc. Symp. Proc.* **356**, 615 (1995).
- ¹³H. S. Ogawa, D. R. McMullin, D. L. Judge, and R. Korde, *Opt. Eng.* **32**, 3121 (1993).
- ¹⁴D. L. Judge, D. R. McMullin, H. S. Ogawa, D. Hovestadt, B. Klecker, M. Hilchenbach, E. Mobius, L. R. Canfield, R. E. Vest, R. Watts, C. Tarrío, M. Kuhne, and P. Wurz, *Sol. Phys.* **177**, 161 (1998).
- ¹⁵J. L. Burch, S. B. Mende, D. G. Mitchell, T. E. Moore, C. J. Pollock, B. W. Reinisch, B. R. Sandel, S. A. Fuselier, D. L. Gallagher, J. L. Green, J. D. Perez, and P. H. Reiff, *Science* **291**, 619 (2001).
- ¹⁶J. L. Burch, *Sci. Am.* **284**, 86 (2001).
- ¹⁷M. Gruntman, *Rev. Sci. Instrum.* **68**, 3617 (1997).
- ¹⁸C. J. Pollock, M. Balkey, J. Burch, J. Cravens, G. Dirks, H. Funsten, M. Grande, M. Gruntman, J.-M. Jahn, M. Lampton, D. J. McComas, T. Mukai, S. Pope, S. Ritzau, E. Scime, M. L. Schattenburg, R. Skoug, P. Valek, S. Weidner, and M. Wuest, *Space Sci. Rev.* **91**, 113 (2000).
- ¹⁹E. E. Scime, E. H. Anderson, D. J. McComas, and M. L. Schattenburg, *Appl. Opt.* **34**, 648 (1995).
- ²⁰M. M. Balkey, E. E. Scime, M. L. Schattenburg, and J. van Beek, *Appl. Opt.* **37**, 5087 (1998).
- ²¹J. van Beek, R. C. Fleming, P. S. Hindle, J. D. Prentiss, S. Ritzau, and M. L. Schattenburg, *J. Vac. Sci. Technol. B* **16**, 3911 (1998).
- ²²C. J. Pollock, K. Asamura, M. M. Balkey, J. L. Burch, H. O. Funsten, M. Grande, M. Gruntman, J.-M. Jahn, M. Lampton, M. W. Liemohn, D. J. McComas, T. Mukai, S. Ritzau, M. L. Schattenburg, E. Scime, R. Skoug, P. Valek, and M. Wüest, *Geophys. Res. Lett.* **8**, 1147 (2001).
- ²³T. S. Molinski, W. E. Ferro, and B. L. Damski, *IEEE Spectrum* **37**, 55 (2000).
- ²⁴T. Savas, M. L. Schattenburg, J. M. Carter, and H. I. Smith, *J. Vac. Sci. Technol. B* **14**, 4167 (1996).
- ²⁵A. E. Franke, M. L. Schattenburg, E. M. Gullikson, J. Cottam, S. M. Kahn, and A. Rasmussen, *J. Vac. Sci. Technol. B* **15**, 2940 (1997).
- ²⁶M. L. Schattenburg, C. Chen, P. N. Everett, J. Ferrera, P. Konkola, and H. I. Smith, *J. Vac. Sci. Technol. B* **17**, 2692 (1999).
- ²⁷C. G. Chen, P. T. Konkola, R. K. Heilmann, G. S. Pati, and M. L. Schattenburg, *J. Vac. Sci. Technol. B*, these proceedings.
- ²⁸C. J. Hailey, S. Abdali, F. E. Christensen, W. W. Craig, T. R. Decker, F. A. Harrison, and M. Jimenez-Garate, *Proc. SPIE* **3114**, 535 (1997).
- ²⁹C. G. Chen, R. K. Heilmann, P. T. Konkola, O. Mongrard, G. P. Monnelly, and M. L. Schattenburg, *J. Vac. Sci. Technol. B* **18**, 3272 (2000).
- ³⁰G. P. Monnelly, O. Mongrard, D. Breslau, N. Butler, C. G. Chen, L. Cohen, W. Gu, R. K. Heilmann, P. T. Konkola, G. R. Ricker, and M. L. Schattenburg, *Proc. SPIE* **4138**, 164 (2000).
- ³¹H. Bergner, L. M. Cohen, M. L. Schattenburg, and G. Monnelly, *Proc. SPIE* **4138**, 134 (2000).
- ³²P. J. Serlemitsos *et al.*, *Publ. Astron. Soc. Jpn.* **47**, 105 (1995).
- ³³J. E. Harvey, E. C. Moran, and W. O. Zmek, *Appl. Opt.* **27**, 1527 (1988).
- ³⁴N. White, *Nature (London)* **407**, 146 (2000).